JOURNAL OF SPACECRAFT AND ROCKETS
Vol. 50, No. 1, January–February 2013

Gravity Error Compensation Using Second-Order Gauss–Markov Processes

Jason M. Leonard,* Felipe G. Nievinski,† and George H. Born‡
University of Colorado, Boulder, Colorado 80309

DOI: 10.2514/1.A32262

Earth science satellite missions currently require orbit determination solutions with position accuracies to within a centimeter. The estimation of empirical accelerations has become commonplace in precise orbit determination for Earth-orbiting satellites. Dynamic model compensation uses an exponentially time-correlated system noise process, known as a first-order Gauss–Markov process, to estimate unmodeled accelerations. In this work, the use of a second-order Gauss–Markov process is addressed to compensate for higher order spherical harmonic gravity accelerations, beyond J_3. Improvements in precise orbit determination and orbit prediction through the implementation of an optimal second-order Gauss–Markov process for empirical acceleration estimation are assessed. The use of a single well-calibrated second-order Gauss–Markov process outperforms a first-order Gauss–Markov process and a poorly calibrated second-order Gauss–Markov process for both continuous observations and poor tracking data.

Nomenclature

$\mathbf{A}$	=	Jacobian matrix
$\mathbf{B}$	=	process noise mapping matrix
c	=	process noise coefficient
E	=	expectation operator
$\mathbf{F}$	=	dynamic model
$\mathbf{G}$	=	observation model
$\tilde{\mathbf{H}}$	=	observation-state mapping matrix
$\mathbf{I}$	=	identity matrix
i	=	imaginary number
$\mathbf{n}$	=	dynamic noise
$\mathbf{P}$	=	variance–covariance matrix
$\mathbf{Q}$	=	process noise covariance matrix
q	=	white noise strength
$\mathbf{r}$	=	position vector, m
$\dot{\mathbf{r}}$	=	velocity vector, m/s
$\ddot{\mathbf{r}}$	=	acceleration vector, m/s^2
T	=	correlation time, s
t	=	time, s
$\mathbf{w}$	=	Gaussian noise
$\mathbf{X}$	=	state vector
$\dot{\mathbf{X}}$	=	state-rate vector
$\mathbf{x}$	=	linearized state vector
$\dot{\mathbf{x}}$	=	linearized state-rate vector
$\mathbf{Y}$	=	observation vector
$\mathbf{y}$	=	linearized observation vector
β	=	damped frequency
$\boldsymbol{\beta}$	=	state parameter matrix
$\dot{\boldsymbol{\beta}}$	=	state-rate parameter matrix
δ	=	Dirac delta
$\boldsymbol{\epsilon}$	=	observation noise
ζ	=	damping coefficient
λ	=	time constant
σ	=	noise variance
τ	=	time shift, s
Φ	=	state transition matrix
Ψ	=	autocovariance, m^2/s^4
ω	=	angular frequency, rad/s
ω_n	=	natural frequency, rad/s

Subscripts

a	=	augmented filter
d	=	discrete filter
s	=	shaping filter
x	=	inertial X direction
y	=	inertial Y direction
z	=	inertial Z direction
0	=	initial condition

I. Introduction

OCEANOGRAPHIC and geodetic Earth science satellite missions currently require orbit determination solutions with position accuracies to within a centimeter [1]. High-accuracy requirements demand commensurate mathematical models of orbital dynamics. Regardless of the accuracy of these mathematical models, however, there will always be unknown accelerations acting upon a spacecraft. The estimation of empirical accelerations has become commonplace in precise orbit determination (POD) for Earth-orbiting satellites [1–3].

Empirical acceleration estimation methods are more commonly known as reduced dynamic modeling (RDM) [2,3]. Several methods exist to estimate these unmodeled accelerations. One such method attempts to estimate periodic accelerations with trigonometric coefficients at fixed frequencies [1,4]. Another, called dynamic model compensation, uses an exponentially time-correlated system noise process, known as a first-order Gauss–Markov process (GMP1) [5–7]. A third option lies in physically based autocovariance models describing errors of commission and omission in gravity [8–11]. A fourth variant exists in batch estimation, where piecewise-constant time-dependent accelerations can be included as unknown parameters [12]. Nazarenko and Alfriend [13] developed an approach for estimating the colored noise parameters in the orbit determination process for correlation functions of gravity disturbing forces.

It could be argued that the mathematical formulation of a second-order Gauss–Markov process (GMP2) is well known in the control literature [14–16]. Yet GMP2s are not employed for routine POD as widely as they perhaps deserve to be. As an initial proof-of-concept, Nievinski et al. [17] demonstrated an improvement in POD through the use of GMP2 for modeling J_3 gravity. This was made possible by the fact that GMP2 allows a more flexible autocovariance model with both exponential decay and sinusoidal oscillation properties.

Received 21 October 2011; revision received 1 March 2012; accepted for publication 7 March 2012.

*Graduate Research Assistant, Department of Aerospace Engineering.
†Ph.D. Student, Department of Aerospace Engineering.
‡Professor, Department of Aerospace Engineering Sciences and Director, Colorado Center for Astrodynamics Research.

The capability of GMP2 for modeling random, approximately oscillatory phenomena makes it adequate in accounting for a variety of accelerations that tend to repeat as a function of satellite orbital revolution, such as gravity, atmospheric drag, and solar radiation pressure. GMP2 could serve as a generic replacement for more specialized, physically based autocovariance models, not to mention accounting for accelerations lacking a more rigorous autocovariance description [9–11]. GMP2 offers a more flexible autocovariance model, which embraces and extends the two extremes typically adopted in RDM, between a pure exponential decay and a pure sinusoidal oscillation.

In this work, several GMP methods are compared for compensating higher order spherical harmonic gravity accelerations, beyond J_2. A derivation of GMPs is also provided. The problem of calibrating the coefficients driving the stochastic model for GMP is addressed. Thirdly, position and acceleration estimation results are presented for two orbits over two different tracking regimes. Finally, an introduction to compound GMP2 is presented, as used for gravity error compensation.

II. Filter Theory

A. Sequential Filter

The following derivation outlines the sequential filter. The state vector is denoted by $\mathbf{X}(t)$ and contains the satellite position and velocity coordinates as well as parameters governing accelerations acting on the satellite, such as gravity and atmospheric drag coefficients. The dynamic model and observation model are, respectively,

$$\dot{\mathbf{X}}(t) = \mathbf{F}(\mathbf{X}, t) \tag{1}$$

$$\mathbf{Y}(t) = \mathbf{G}(\mathbf{X}, t) \tag{2}$$

These models are then linearized about their reference trajectory (denoted with an asterisk) by

$$\dot{\mathbf{x}}(t) = \mathbf{A}(t)\mathbf{x}(t) + \mathbf{B}(t)\mathbf{n}(t) \tag{3}$$

$$\mathbf{y}(t) = \tilde{\mathbf{H}}(t)\mathbf{x}(t) + \boldsymbol{\epsilon}(t) \tag{4}$$

where $\mathbf{x}(t) = \mathbf{X}^*(t) - \mathbf{X}(t)$ and $\dot{\mathbf{x}}(t) = \dot{\mathbf{X}}^*(t) - \dot{\mathbf{X}}(t)$. Here, $\mathbf{n}(t)$ and $\boldsymbol{\epsilon}(t)$ are the dynamic and observation noise, respectively, and $\mathbf{B}(t)$ is the process noise mapping matrix. The matrix $\mathbf{A}(t)$ is evaluated along the reference trajectory $\mathbf{X}^*(t)$ and is given by

$$\mathbf{A}(t) = \frac{\partial \mathbf{F}(\mathbf{X}^*, t)}{\partial \mathbf{X}} \tag{5}$$

The state transition matrix $\Phi(t, t_0)$ is related to $\mathbf{A}(t)$ by

$$\dot{\Phi}(t, t_0) = \mathbf{A}(t)\Phi(t, t_0) \tag{6}$$

The observation-state mapping matrix is thus given by

$$\tilde{\mathbf{H}}(t) = \frac{\partial \mathbf{G}(\mathbf{X}^*, t)}{\partial \mathbf{X}} \tag{7}$$

where $\mathbf{G}(\mathbf{X}^*, t)$ are the observation-state relationships evaluated on the reference trajectory.

B. Shaping Filter

There are many cases in which a commonly employed white Gaussian noise model does not describe the system dynamic noise adequately. It would be more desirable to have a model that could match the empirical autocovariance or power spectral density data of an observed system, and then generate a stochastic mathematical model to reproduce the empirical characteristics. If an observed set of data were samples of a stationary Gaussian process with known autocovariance (or power spectral density), then a linear time-invariant system, or shaping filter, driven by white Gaussian noise, could provide such a model [16]. Moreover, it is often the case that only the first- and second-order statistics are known, for which a Gaussian process with the same first- and second-order statistics can be generated by a shaping filter.

The system dynamics were defined earlier by Eqs. (3) and (4) where the observation noise $\boldsymbol{\epsilon}(t)$ is postulated uncorrelated and the dynamic noise $\mathbf{n}(t)$ is a colored, time-correlated, dynamic Gaussian noise. The latter is obtained by passing a white Gaussian noise $\mathbf{w}(t)$ through a shaping filter defined by

$$\dot{\mathbf{x}}_s(t) = \mathbf{A}_s(t)\mathbf{x}_s(t) + \mathbf{B}_s(t)\mathbf{w}(t) \tag{8}$$

$$\mathbf{y}_s(t) = \tilde{\mathbf{H}}_s(t)\mathbf{x}_s(t) \tag{9}$$

where the shaping filter output $\mathbf{y}_s(t) = \mathbf{n}(t)$ is used to drive the system defined by Eq. (3). An augmented state vector $\mathbf{x}_a(t)$ is then defined through

$$\mathbf{x}_a(t) = \begin{bmatrix} \mathbf{x}(t) \\ \mathbf{x}_s(t) \end{bmatrix} \tag{10}$$

where the augmented state equation is given by

$$\begin{bmatrix} \dot{\mathbf{x}}(t) \\ \dot{\mathbf{x}}_s(t) \end{bmatrix} = \begin{bmatrix} \mathbf{A}(t) & \mathbf{B}(t)\tilde{\mathbf{H}}_s(t) \\ \mathbf{0} & \mathbf{A}_s(t) \end{bmatrix} \begin{bmatrix} \mathbf{x}(t) \\ \mathbf{x}_s(t) \end{bmatrix} + \begin{bmatrix} \mathbf{0} \\ \mathbf{B}_s(t) \end{bmatrix} \mathbf{w}(t) \tag{11}$$

or

$$\dot{\mathbf{x}}_a(t) = \mathbf{A}_a(t)\mathbf{x}_a(t) + \mathbf{B}_a(t)\mathbf{w}(t) \tag{12}$$

and its associated output equation

$$\begin{aligned} \mathbf{y}_a(t) &= \begin{bmatrix} \tilde{\mathbf{H}}(t) & \mathbf{0} \end{bmatrix} \begin{bmatrix} \mathbf{x}(t) \\ \mathbf{x}_s(t) \end{bmatrix} + \boldsymbol{\epsilon}(t) \\ &= \tilde{\mathbf{H}}_a(t) \quad \mathbf{x}_a(t) + \boldsymbol{\epsilon}(t) \end{aligned} \tag{13}$$

C. Time Update

The preceding section developed a set of equations for a linear stochastic system driven by white noise and defined by Eq. (12). It is possible to interpret it as a linear stochastic differential equation of the form

$$\mathrm{d}\,\mathbf{x}_a(t) = \mathbf{A}_a(t)\mathbf{x}_a(t)\,\mathrm{d}t + \mathbf{B}_a(t)\,\mathrm{d}\mathbf{w}(t) \tag{14}$$

whose solution is

$$\mathbf{x}_a(t) = \Phi_a(t, t_0)\mathbf{x}_a(t_0) + \int_{t_0}^{t} \Phi_a(t, t')\mathbf{B}_a(t')\,\mathrm{d}\mathbf{w}(t') \tag{15}$$

where $\Phi_a(t, t_0) = \partial \mathbf{X}_a(t)/\partial \mathbf{X}_a(t_0)$ and the statistical expectation $\mathrm{E}\{\mathbf{x}_a(t)\} = 0$. Also, the stochastic integral of the white Gaussian noise process is implicitly independent of $\mathbf{x}_a(t)$ and, therefore,

$$\mathrm{E}\left\{\left[\int_{t_0}^{t} \Phi_a(t, t')\mathbf{B}_a(t')\,\mathrm{d}\mathbf{w}(t')\right][\mathbf{x}_a(t)]\right\} = 0 \tag{16}$$

thus the time update for the state $\mathbf{x}_a(t)$ is not affected and is simply $\mathbf{x}_a(t) = \Phi_a(t, t_0)\mathbf{x}_a(t_0)$. However, the variance–covariance matrix of $\mathbf{x}_a(t)$ is affected and has the form

$$\begin{aligned} \bar{\mathbf{P}}_a(t) &= \Phi_a(t, t_0)\mathbf{P}_a(t_0)\Phi_a^{\mathrm{T}}(t, t_0) \\ &\quad + \int_{t_0}^{t} \Phi_a(t, t')\mathbf{B}_a(t')\mathbf{Q}_a(t')\mathbf{B}_a^{\mathrm{T}}(t')\Phi_a^{\mathrm{T}}(t, t')\,\mathrm{d}t' \end{aligned} \tag{17}$$

$$\dot{\mathbf{P}}_a(t) = \mathbf{A}_a(t)\bar{\mathbf{P}}_a(t) + \bar{\mathbf{P}}_a(t)\mathbf{A}_a^{\mathrm{T}}(t) + \mathbf{B}_a(t)\mathbf{Q}_a(t)\mathbf{B}_a^{\mathrm{T}}(t) \tag{18}$$

This relationship allows for a time-varying system model and nonwhite, time-correlated, dynamic Gaussian noise model to be evaluated. Two possible methods of solution exist for nontrivial dynamics: numerical integration of Eq. (18), or a discrete case for

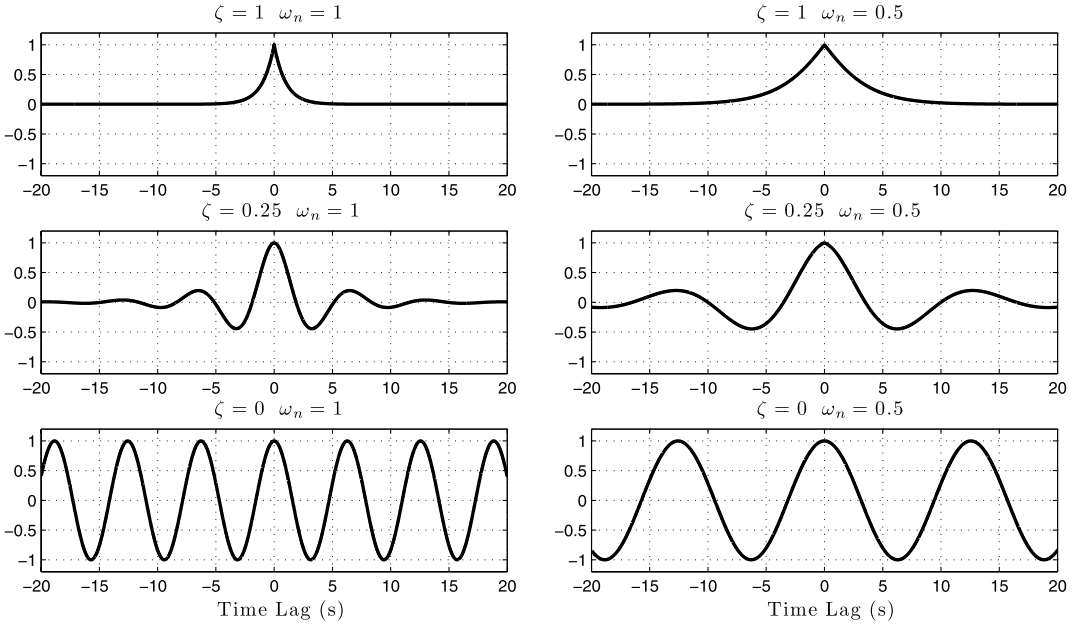

Fig. 1 Autocovariance functions for different instances of second-order GMP.

time-invariant or slowly varying system models based on Eq. (17). For the derivation of the discrete case, [16] is closely followed:

$$\bar{\mathbf{P}}_a(t) = \Phi_a(t,t_0)\mathbf{P}_a(t_0)\Phi_a^{\mathrm{T}}(t,t_0) + \mathbf{B}_d(t_0)\mathbf{Q}_d(t_0)\mathbf{B}_d^{\mathrm{T}}(t_0) \tag{19}$$

where the subscript d denotes the discrete case to distinguish it from the instantaneous case presented earlier (see Appendix B for matrices $\mathbf{B}_d$ and $\mathbf{Q}_d$). If the system model natural transients are time-invariant or slowly varying when compared with the observation samples, then a first-order approximation can be used, where

$$\Phi_a(t,t_0) = \mathbf{I} - \mathbf{A}_a(t_0) \times (t - t_0) \tag{20}$$

$$\mathbf{Q}_d(t_0) = \mathbf{B}_a(t_0)\mathbf{Q}_a(t_0)\mathbf{B}_a^{\mathrm{T}}(t_0) \times (t - t_0) \tag{21}$$

III. Gauss–Markov Theory

A Gauss–Markov random process is a Markov random process with restriction that the probability $p[x(t)]$ and the conditional probability $p[x(t)/x(t+\tau)]$, where $\tau = \Delta t$, are Gaussian density functions for all times t and $t+\tau$ over the interval $t_0 \to t_f$ [15]. In terms of filter theory, a zeroth-, first-, and second-order process (GMP0, GMP1, GMP2) augment the state vector with zero, one, or two parameters, respectively, per spatial dimension [17]. For any scalar zero-mean noise process, the autocovariance is defined as

$$\Psi_{nn}(\tau) = \mathrm{E}\{n(t)n(t+\tau)\} \tag{22}$$

Pure white noise is defined by a GMP0 whose autocovariance function is represented by

$$\Psi_{nn}(\tau) = \sigma^2\delta(\tau) \tag{23}$$

where σ^2 is the noise variance corresponding to $\tau = 0$, and δ is the Dirac delta function. GMP1 is defined by an exponentially correlated function with a correlation time T, where $\lambda = 1/T$, and an autocovariance

$$\Psi_{nn}(\tau) = \sigma^2 e^{-\lambda\tau} \tag{24}$$

GMP1 is also defined by the first-order Langevin equation of the form[§]

$$\dot{n}(t) = -\lambda n(t) + w(t) \tag{25}$$

$$\mathrm{E}\{w(t)\} = 0, \qquad \mathrm{E}\{w(t)w(t+\tau)\} = Q\delta(\tau) \tag{26}$$

The second-order Gauss–Markov process is defined by an autonomous second-order dynamic system with a white noise forcing function of the type[¶]

$$\begin{bmatrix}\dot{x}_1\\ \dot{x}_2\end{bmatrix} = \begin{bmatrix}0 & 1\\ -\omega_n^2 & -2\zeta\omega_n\end{bmatrix}\begin{bmatrix}x_1\\ x_2\end{bmatrix} + \begin{bmatrix}0\\ c\end{bmatrix}w(t) \tag{27}$$

$$\mathrm{E}\{w(t)\} = 0, \qquad \mathrm{E}\{w(t)w(t+\tau)\} = q\delta(\tau) \tag{28}$$

where ω_n, ζ, and c are constants.[**] The strength of the white noise process is generally taken to be $q = 1$ and can be increased to add more noise. The state transition matrix for Eq. (27) is easily obtained:

$$\Phi_s(t) = e^{-\zeta\omega_n t}\begin{bmatrix}\cos\beta t + \frac{\zeta\omega_n}{\beta}\sin\beta t & \frac{1}{\beta}\sin\beta t\\ -\frac{\omega_n^2}{\beta}\sin\beta t & \cos\beta t - \frac{\zeta\omega_n}{\beta}\sin\beta t\end{bmatrix} \tag{29}$$

where, $\beta = \omega_n\sqrt{1-\zeta^2}$. From Eq. (17) with $\mathbf{B}_s = [0, \quad c]^{\mathrm{T}}$, the autocovariance function for a GMP2 is given by [15,18]

$$\Psi_{nn}(\tau) = \sigma^2 e^{-\zeta\omega_n|\tau|}\left\{\cos\beta|\tau| + \frac{\zeta\omega_n}{\beta}\sin\beta|\tau|\right\} \tag{30}$$

where $\sigma^2 = qc^2/4\omega_n^3\zeta$ (see Appendix A for details). This formula will always be written for the underdamped case; for the aperiodic case, let $\beta \to 0$, and for the overdamped case, set $\beta = i\beta$ [18].

Figure 1 illustrates the versatility of the GMP2 autocovariance function as see in Eq. (30). From GMP2, one can obtain GMP0, GMP1, and a pure sinusoid by altering the coefficients ω_n and ζ. For example, if $\zeta = 1$, it degenerates into GMP1 with a pure exponential

[§]One must be made aware that Q in Eq. (26) and q in Eq. (28) are the strengths of a white noise process but may have different units and are thus defined differently. Also σ^2 in Eq. (23) $\neq Q$ or q but can also be defined as the strength of a white noise process for GMP0.

[¶]Notice that [17] followed [16], yet here [15] and [18] are followed; these two are not exactly equivalent, especially in Eqs. (27), (30), and (B7). Furthermore, there was a typo in [17], Eq. 16, where it is b, but should be c.

[**]In [17], $\omega_n = \omega$ and c is a variable different than the constant defined here.

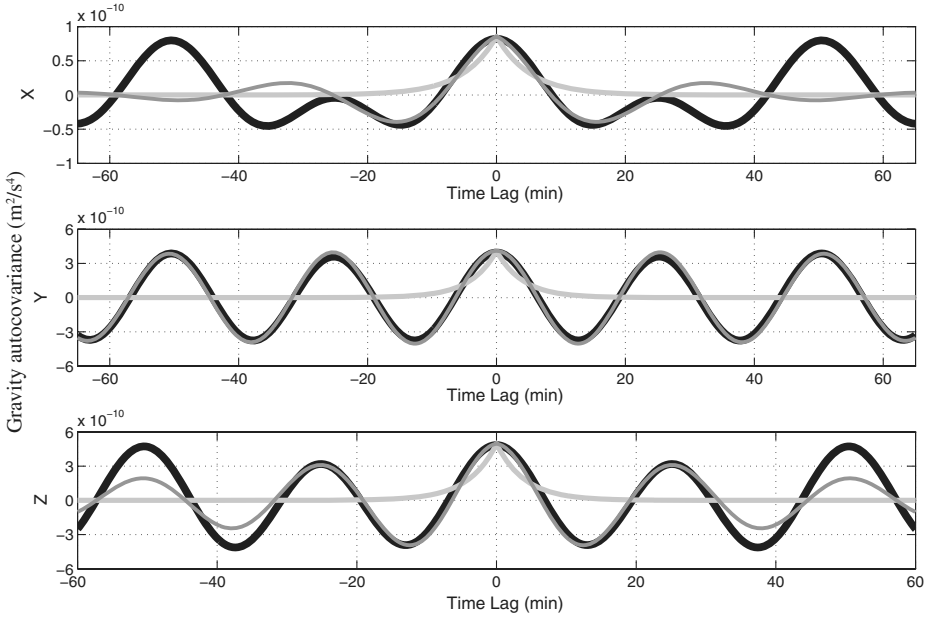

Fig. 2 J3 ECI acceleration autocovariance (black) with GMP1 (light gray), restrained GMP2 (dark gray) fits.

decay. On the other extreme, $\zeta = 0$ leads to a pure sinusoidal oscillation. The frequencies are governed by ω_n and if $\zeta = 1$ with $\omega_n \to \infty$, approaching the solution of GMP0.

IV. Method

A. Models

A set of range and range-rate observations are generated from a space-borne geostationary (GEO) tracking network (three GEO tracking satellites separated by 120 degrees) using true equations of motion that are corrupted by white Gaussian noise with a standard deviation of 0.1 m and 0.01 m/s, respectively. An estimate of the true state of the satellite is obtained by an inversion of such simulated observations through a conventional Kalman filter. The spacecraft state vector is expressed in an Earth-centered inertial (ECI) coordinate system, where the X-Y plane coincides with the Earth equatorial plane, and the X and Z axes directed toward the mean equinox and north pole, respectively.

Two low-Earth-orbit (LEO) cases were considered: Case 1 is a typical LEO satellite; case 2 is based on a Jason-1-type orbit. Simulated true equations of motion are integrated with an efficient seventh-order Runge–Kutta–Fehlberg RKF7(8) algorithm [19]. The true equations of motion include acceleration of the Earth's spherical and nonspherical gravitational field, as well as atmospheric drag. The evaluation of the Earth's gravitational acceleration is taken from the GRACE gravity model (GGM02C) [20] for spherical harmonic terms up to degree and order 100 using the normalized Cartesian model [21]. A simple drag model with a spherical body was used. The atmospheric density is given by the U.S. Naval Research Laboratory Mass Spectrometer and Incoherent Scatter Radar (NRLMSISE-00) model [22].

The filter equations of motion consist of the Earth central body and oblateness (J_2) with atmospheric drag and a term for unmodeled accelerations (expressed as either a GMP1 or GMP2). The reduced filter equations of motion provide a mismatch in the dynamic model between the filter and truth, allowing for GMPs to compensate for the dynamic model errors and recover the higher order gravity harmonics (see Appendix B for filter implementation). Calibration for the GMP coefficients σ^2, ω_n, and ζ is done using the method presented next.

B. Calibration

It must be assumed that the GMP coefficients [σ, ζ, and ω_n in Eq. (30)] are known during the filter runs. Here the problem of calibrating such coefficients is addressed. Calibration of the coefficients can be a problem and is addressed in a three-step procedure: 1) obtain sample accelerations, 2) form covariances, and 3) fit autocovariance model to samples.

This calibration or tuning is usually addressed under the name of "adaptive filtering or estimation" [23–26]. The following calibration analysis uses a typical LEO satellite in which J_3 is the unmodeled acceleration to be recovered. The procedure outlined in this section is the same as the calibration method used in the following cases, although the acceleration itself is different. Step 1 is the most difficult one, and so the others will be briefly addressed first.

Step 3, fitting model Eq. (30) to the samples as seen in Fig. 2, can be done in at least three ways: 3.a) manually, or 3.b) automatically, via a nonlinear optimization routine, or 3.c) via ad-hoc methods. Step 3.a involves trial and error, thus it is admittedly a pedestrian method. But it is undoubtedly feasible and even efficient, in a typical usage scenario. After all, with a single satellite mission of interest, its calibration needs to be performed only once. Furthermore, solutions from the simpler 3.a may serve as good initial solutions for the more complicated method 3.b, enabling or at least speeding up convergence in the latter. Thus 3.b is especially valuable in refining preexisting approximate solutions. Although 3.b is in principle complicated, its utilization is facilitated by the possibility of treating the model Eq. (30) as a black box. That way, its partial derivatives (with respect to the coefficients) are obtained numerically. Although this is more computationally intensive, it is certainly less tedious and also less error prone, compared with analytical Jacobians. All other methods fall under the umbrella of 3.c; these include, but are not limited to, for example, spectral analysis to identify peak frequencies thus ω_n, sample standard deviation to obtain σ, and finite differencing or curve fitting near the origin to approximate ζ.

Step 2, forming covariances is trivial given sample accelerations regularly spaced in time. This can be accomplished simply as $\mathrm{IFFT}(|\mathrm{FFT}(s)| \cdot |\mathrm{FFT}(s)|)$, where s is a vector of sample accelerations, $|\cdot|$ is the elementwise complex modulus, $\cdot$ is the elementwise product, and FFT/IFFT are the fast Fourier transform and its inverse. For better methods, especially more accurate normalizations, please refer to [27]. When accelerations are not sampled at regular time intervals, forming the autocovariance is more laborious. It can be done as follows. Collect the time of each sample in an $n \times 1$ vector $t = [t_k]$. Form the time-lag matrix as $T = \mathrm{abs}([t, t, \ldots, t]_{n\times n} - [t, t, \ldots, t]^{\mathrm{T}}_{n\times n})$, which is symmetric, with zeros in the main diagonal. Construct the corresponding sample covariance matrix $S = ss^T$, where $s = [s_k]$ is the sample vector. The so-called sample covariance cloud can be obtained plotting points with T_{ij} as

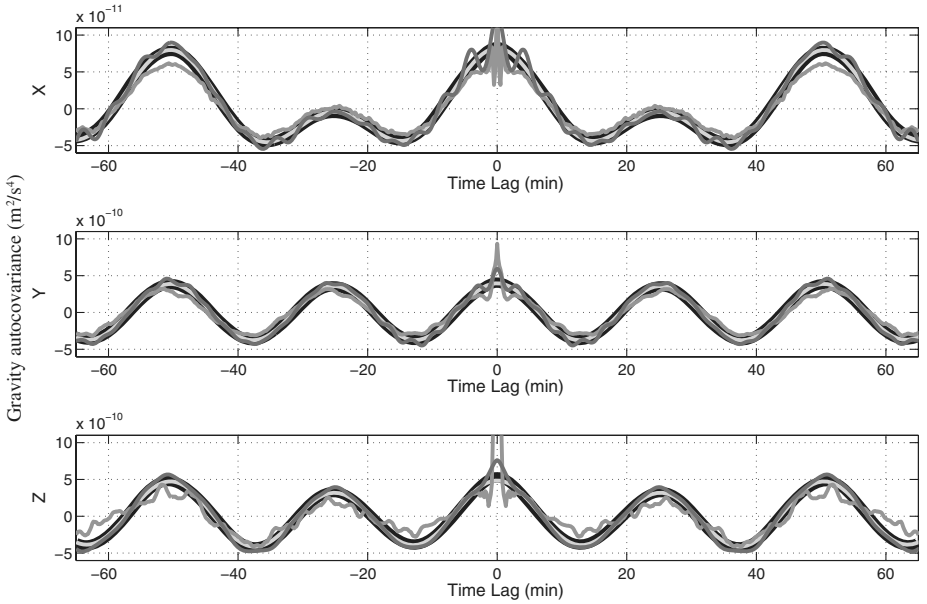

Fig. 3 J3 ECI acceleration autocovariance, based on predictive physical model (black) and on different GMP1-estimated sample accelerations: well-calibrated, backward smoothed (light gray), well-calibrated, forward-filtered only (medium gray), and poorly calibrated, backward smoothed (dark gray).

abscissa and S_{ij} as ordinate, that is, made of corresponding elements in the two matrix. Finally, the sample covariance function can then be found binning the cloud by time lag at regular intervals $\tau = [\tau_l]$, that is, $C_l = \sum S_{qr}/N_l$, where N_l is the number of samples within that bin, and the binning criteria yields q, r indices such that $(\tau_{l-1} + \tau_l)/2 < T_{qr} < (\tau_l + \tau_{l+1})/2$. In either case (regular or irregularly spaced), it is important to have a sufficiently long sample vector, because the autocovariance behavior at large time lags is more poorly determined (i.e., there are less numerous pairs of samples separated by larger time lags).

Now returning to the main step (step 1), sample accelerations can be obtained as predictions given by a physical model (over a nominal satellite orbit) or as estimates from a preliminary filter run. Predictive physical models can be, for example, an expansion of the gravity potential in spherical harmonics, a climatology of atmospheric density, etc. The other option is a hard problem: Given tracking data only, it seeks to bootstrap the optimal filter calibration, starting from a suboptimal one. The filter is ran first with best guesses about σ, ω_n, ζ; the resulting preliminary acceleration samples are then fed into step 2 and then step 3. This three-step calibration procedure is iterated until convergence. In general, there is no guarantee that such a bootstrapping will converge to an unbiased solution. Its reliability depends heavily on the sensitivity of the sample accelerations to the coefficient values. Notice that this also involves the quantity and quality of tracking data. In other words, it depends on how well constrained the estimation of empirical accelerations is. For example, sufficiently precise observations could compensate for a loose stochastic constraint in the preliminary filter runs.

To investigate the difficulty in performing the calibration step 1, Fig. 3 compared the model-predicted J_3 acceleration autocovariance (taken as truth) to different estimated sample autocovariances. A well-calibrated and well-observed GMP1 (as in the preceding numerical experiments) performed remarkably well when it was backward smoothed. When the same GMP1 was forward filtered only, though, it failed to capture the correct degree of continuity near the origin (its performance remained decent at larger time lags). Thus backward smoothing seems mandatory for bootstrapping the GMP calibration. A backward-smoothed well-observed, but poorly calibrated GMP1 was also tested, meaning one with ω_n assuming 10 times its optimal value. Its performance is decidedly better than that of a well-calibrated but forward-filtered only solution, across the whole range of time lags. Nevertheless, the behavior near the origin was again severely degraded. This seems to suggest that the degree of continuity near the origin is hard to infer from tracking data alone; it would be more reliable to constrain it based on a physical justification. On a more encouraging tone, notice that the accuracy demanded from a predictive model is less stringent in the GMP calibration, compared with using the same predictive model as part of the dynamic model. The reason is that, whereas in the latter usage needs the expected value of acceleration at instantaneous epochs, the former only needed to know how accelerations remain correlated over increasing time lags.

V. Results

Position and acceleration estimation results are presented for two cases over two different tracking regimes: constant tracking every 10 s, and random loss of tracking 90% of the time. Before filter convergence, the first 20 min of every filter run is ignored when computing the statistics.

A. Case 1

Case 1 is an eccentric orbit with a perigee/apogee height of 160/380 km, an inclination of 110 deg, argument of perigee of 130 deg, and an orbital period of about 90 min. This satellite experiences a highly variable acceleration and autocovariance function and is a typical LEO satellite. A single GMP1 and two individual GMP2s (restrained GMP2a and unrestrained GMP2b) are fit to the autocovariance of estimated unmodeled accelerations as seen in Fig. 4 from an initial filter calibration run. A restrained autocovariance fit models only small time lags, whereas an unrestrained fit tries to model larger time lags. Figure 5 shows filtered acceleration results for a period of constant tracking. Both GMP1 and GMP2 follow the actual acceleration closely.

Table 1 summarizes the statistics for this filter run. The GMP2 outperforms GMP1 by up to 35%. The GMP2b ECI Y coordinate estimation is the worst and can be explained by the poor unrestrained fit near the origin of the autocovariance as seen in Fig. 4. A better fit is obtained by restraining the calibration of the GMP2 for an optimal fit near the origin instead of attempting to pick up all transients over the full time lag. Here the GMP2a autocovariance model is forced to be optimal on the interval of $|\tau| \leq 30$ min. This is an important lesson when compared with previous work [17], in which it was unclear whether preference should be given to fitting the most variance under the empirical autocovariance function instead of only near the origin.

It is necessary to observe the formal uncertainties associated from the filter run. The steady-state covariance exists after 20 min of observation processing. Table 2 lists the steady-state uncertainties

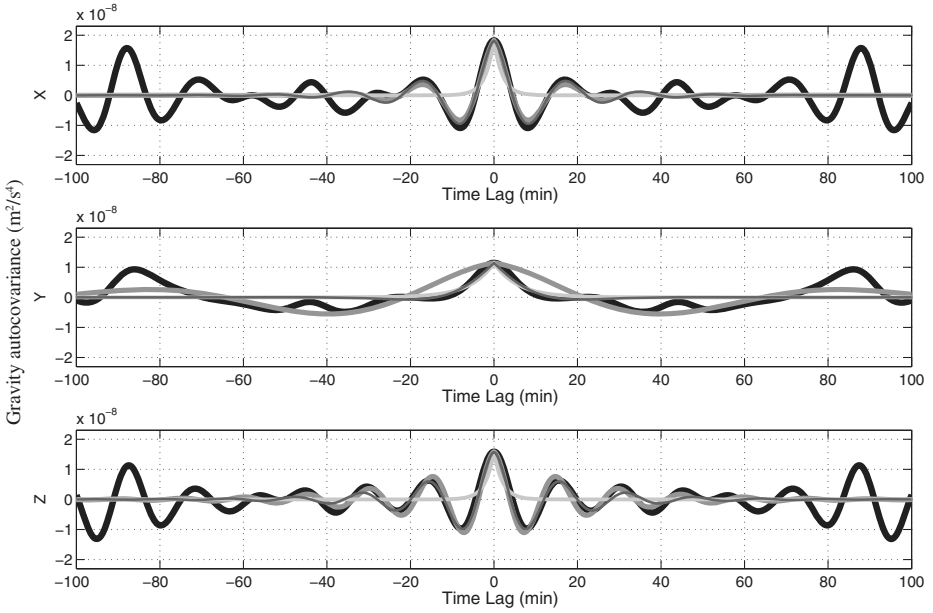

Fig. 4 Case 1 ECI acceleration autocovariance (black) with GMP1 (light gray), restrained GMP2a (dark gray), and unrestrained GMP2b (medium gray) fits.

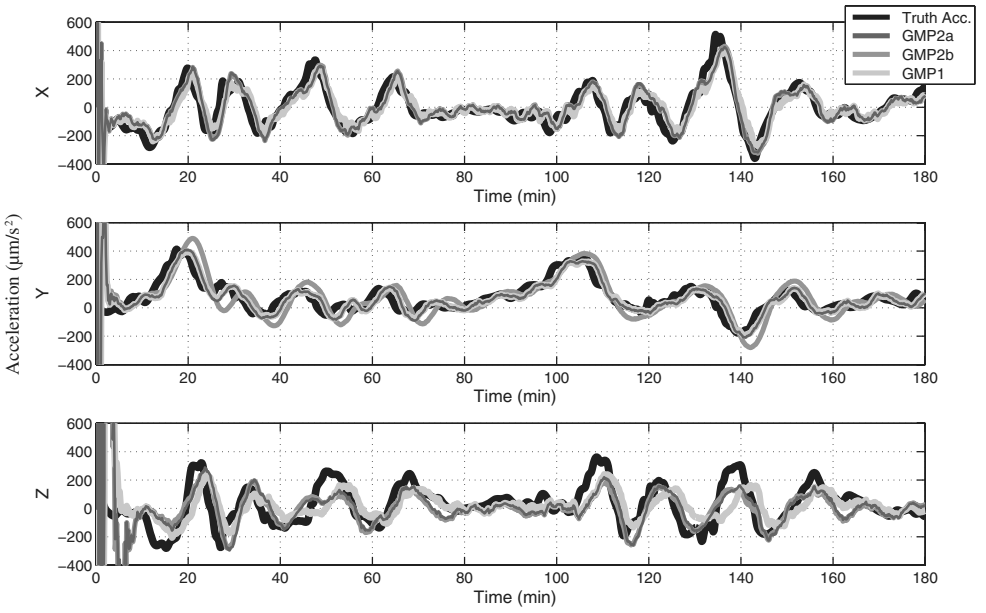

Fig. 5 Case 1 ECI acceleration for fully observed filter run.

determined from the covariance of the filter run. Over 99% of the position and acceleration errors fall within the 3-sigma formal uncertainties for each GMP after the first 20 min. The ECI Z coordinate uncertainty has a periodic oscillation that exists due to the geometry of the problem: The Z coordinate is the least observable from the three GEO tracking satellites. The GMP1 acceleration uncertainty is slightly larger than the GMP2 due to the choice of parameters.

Another filter run is executed as seen in Fig. 6, in which a random loss of tracking throughout the data arc exists. This case experiences roughly the same uncertainties associated with the fully observed one. Table 3 summarizes the statistics for this period. Again, GMP2a

Table 1 Case 1 fully observed period filter rms values[a]

	Position, m			Acceleration, μm/s^2		
	GMP1	GMP2a	GMP2b	GMP1	GMP2a	GMP2b
X	0.076	0.068	0.068	68.11	55.03	54.56
Y	0.079	0.073	0.223	44.50	42.71	73.63
Z	0.865	0.564	0.576	117.32	84.15	87.39
R	0.872	0.573	0.621	142.77	109.25	126.63

[a]Root mean square values are computed from the difference between filtered estimates and true ECI unmodeled accelerations.

Table 2 Case 1 filter steady-state formal uncertainties

3-sigma uncertainty	Position, m			Acceleration, μm/s^2		
ECI Coordinate	GMP1	GMP2a	GMP2b	GMP1	GMP2a	GMP2b
X	1.706	1.254	1.248	355.7	227.4	213.1
Y	1.724	1.141	0.952	189.3	130.8	129.7
Z	6.431	4.519	4.507	402.1	297.6	296.8

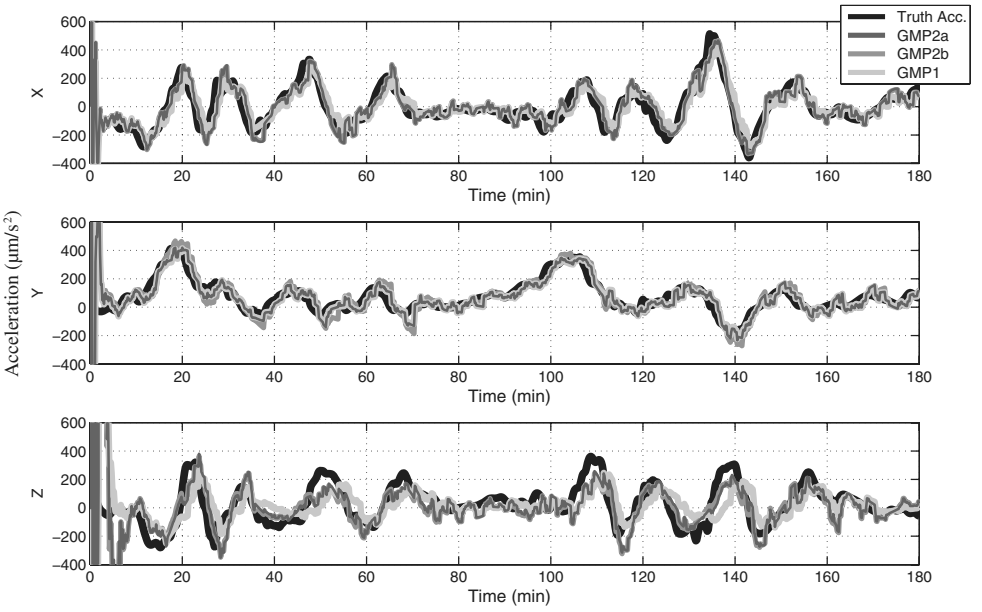

Fig. 6 Case 1 ECI acceleration for partially observed filter run.

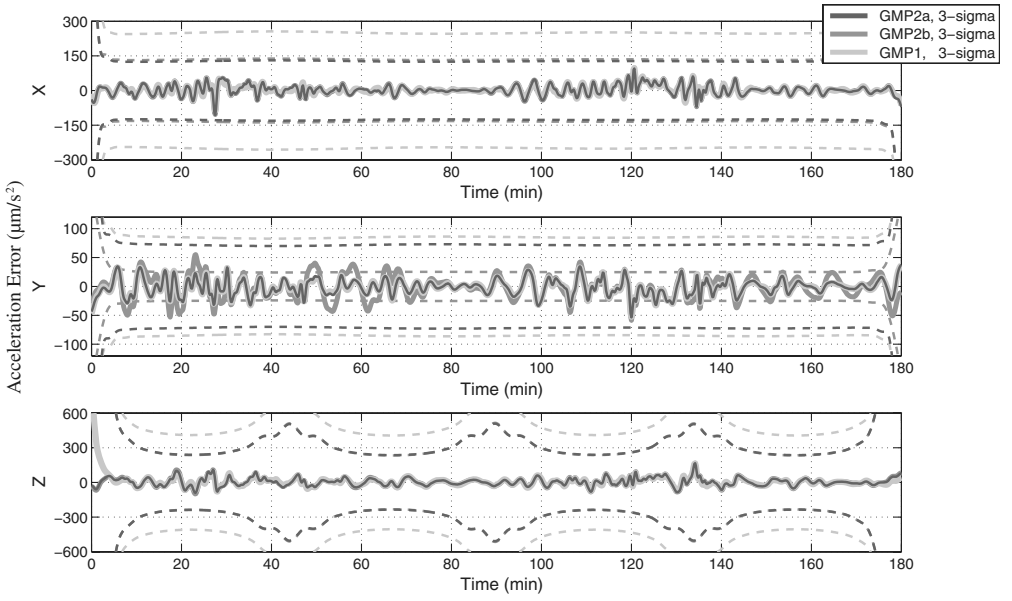

Fig. 7 Case 1 ECI acceleration for fully observed smoothed run.

outperforms GMP1 and GMP2b in acceleration. The *Y* coordinate for GMP2b remains limited by the autocovariance fit near the origin. The *Y* coordinate is challenging even for GMP2a because the empirical autocovariance dies off without the oscillations exhibited in the *X* and *Z* coordinates.

Case 1 is then backward smoothed to determine how well the unmodeled accelerations could be recovered. Figure 7 shows the smoother results for the fully observed case 1 filter run with 3-sigma uncertainty bounds. A majority of the errors are contained within the uncertainty bounds and the GMP1 acceleration uncertainty has been reduced significantly due to smoothing. All three methods recover the unmodeled accelerations rather well, whereas GMP2b is the worst in the *Y* coordinate. Table 4 displays the statistics for the smoothing run. One can see that smoothing has greatly increased

Table 3 Case 1 partially observed period filter rms values[a]

	Position, m			Acceleration, μm/s^2		
	GMP1	GMP2a	GMP2b	GMP1	GMP2a	GMP2b
X	0.206	0.170	0.165	76.97	68.12	67.97
Y	0.153	0.163	0.476	49.32	51.31	89.68
Z	1.345	0.963	0.953	119.12	95.89	99.29
R	1.369	0.991	1.078	150.16	128.33	150.06

[a]Root mean square values are computed from the difference between filtered estimates and true ECI unmodeled accelerations.

Table 4 Case 1 fully observed period smoothed rms values[a]

	Position, m			Acceleration, μm/s^2		
	GMP1	GMP2a	GMP2b	GMP1	GMP2a	GMP2b
X	0.024	0.030	0.030	18.39	20.60	20.27
Y	0.031	0.036	0.118	12.26	12.91	19.17
Z	0.313	0.317	0.314	28.59	31.74	31.94
R	0.316	0.321	0.336	36.14	39.98	42.42

[a]Root mean square values are computed from the difference between smoothed estimates and true ECI unmodeled accelerations

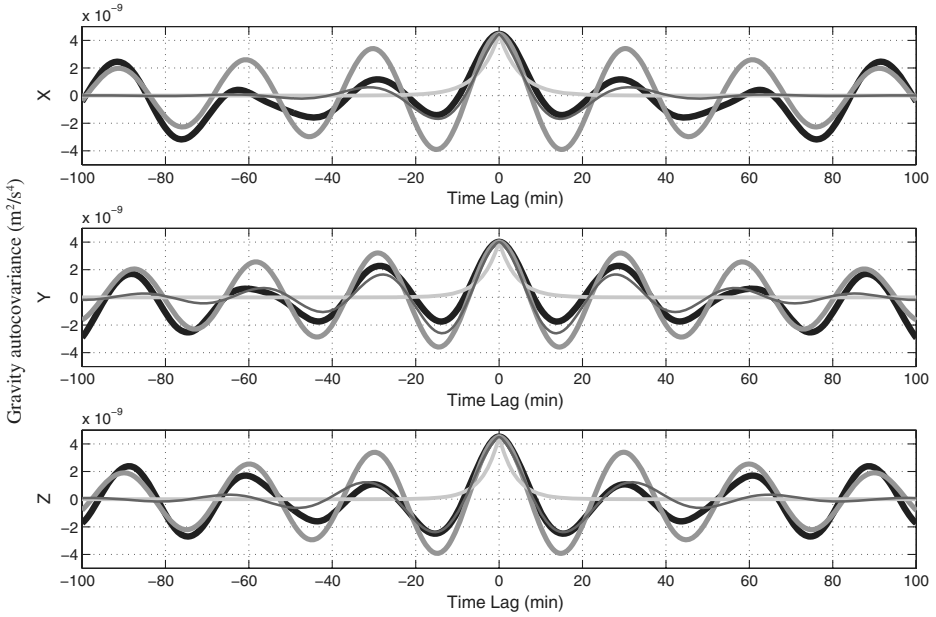

Fig. 8 Case 2 ECI acceleration autocovariance (black) with GMP1 (light gray), restrained GMP2a (dark gray) and unrestrained GMP2b (medium gray) fits.

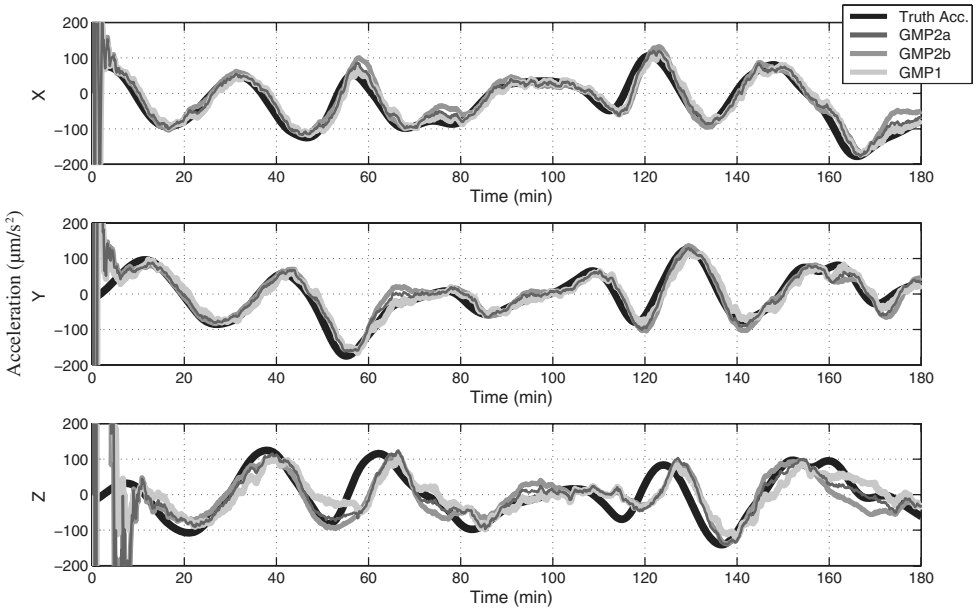

Fig. 9 Case 2 ECI acceleration for fully observed filter run.

the recovery of unmodeled accelerations for case 1. In this case, there is no benefit in using GMP2 in a smoothing run as the smoothed statistics are similar to the GMP1.

B. Case 2

Case 2 is a 1335 km near-circular orbit with an inclination of 66.03 deg, argument of perigee of 23 deg, and an orbital period of about 112 min. This is based on a Jason-1-type orbit in which the autocovariance function is expected to exhibit less variability due to the increased distance from Earth. Similar to case 1, a single GMP1 and two individual GMP2s (restrained GMP2a and unrestrained GMP2b) are fit to the autocovariance of estimated unmodeled acceleration as seen in Fig. 8 from an initial filter calibration run. Here the difference between GMP2a and GMP2b is more drastic in

Table 5 Case 2 fully observed period filter rms values[a]

	Position, m			Acceleration, μm/s^2		
	GMP1	GMP2a	GMP2b	GMP1	GMP2a	GMP2b
X	0.063	0.052	0.082	21.93	17.93	25.26
Y	0.061	0.056	0.082	21.26	17.42	22.75
Z	0.675	0.511	0.820	44.81	38.52	43.48
R	0.680	0.517	0.828	54.23	45.92	55.19

[a]Root mean square values are computed from the difference between filtered estimates and true ECI unmodeled accelerations.

Table 6 Case 2 filter steady-state formal uncertainties

3-sigma uncertainty	Position, m			Acceleration, μm/s^2		
ECI Coordinate	GMP1	GMP2a	GMP2b	GMP1	GMP2a	GMP2b
X	1.628	1.057	0.997	237.2	98.6	61.2
Y	1.568	1.006	0.984	346.8	86.9	57.4
Z	5.521	3.628	3.413	579.3	168.4	108.9

Table 7 Case 2 partially observed period filter rms values[a]

	Position, m			Acceleration, μm/s^2		
	GMP1	GMP2a	GMP2b	GMP1	GMP2a	GMP2b
X	0.139	0.112	0.203	28.04	23.38	33.32
Y	0.132	0.120	0.159	26.66	22.61	28.48
Z	0.922	0.726	1.378	50.07	42.32	47.64
R	0.942	0.745	1.402	63.28	53.38	64.74

[a]Root mean square values are computed from the difference between filtered estimates and true ECI unmodeled accelerations.

all coordinates. Figure 9 shows filtered acceleration results for a period of constant tracking. Again, both GMP1 and GMP2 follow the actual acceleration closely.

Table 5 summarizes the statistics for this. Again, here the GMP2a autocovariance model is forced to be optimal on the interval of $|\tau| \leq 30$ min. The GMP2b autocovariance fit is over the interval of $|\tau| \leq 160$ min, attempting to recovery all transients; this actually does harm to the filter. GMP2a outperforms GMP1 and GMP2b in position and acceleration in all coordinates.

Similar to the preceding case, Table 6 lists the steady-state uncertainties determined from the covariance of the filter run for case 2. Over 99% of the position and acceleration errors fall within the 3-sigma formal uncertainties for each GMP again after the first 20 min. The ECI *Z* coordinate uncertainty has the same periodic oscillation that existed in the preceding case and is due to the geometry of the problem. Here the GMP1 acceleration uncertainty is again larger than the GMP2 uncertainty.

Another filter run is executed as seen in Fig. 10, in which a random loss of tracking throughout the data arc exists. The 3-sigma uncertainties are roughly the same as the fully observed case, reaching steady state after about 20 min, and remaining at the same uncertainties as before. Table 7 summarizes the statistics for this period. For this case, GMP2a outperforms GMP1 and GMP2b in all

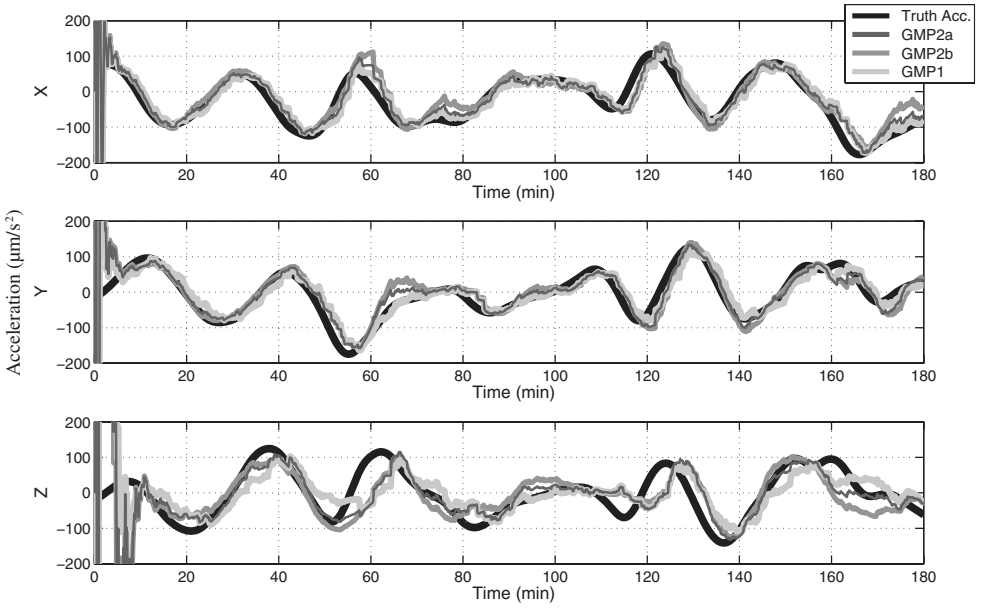

Fig. 10 Case 2 ECI acceleration for partially observed filter run.

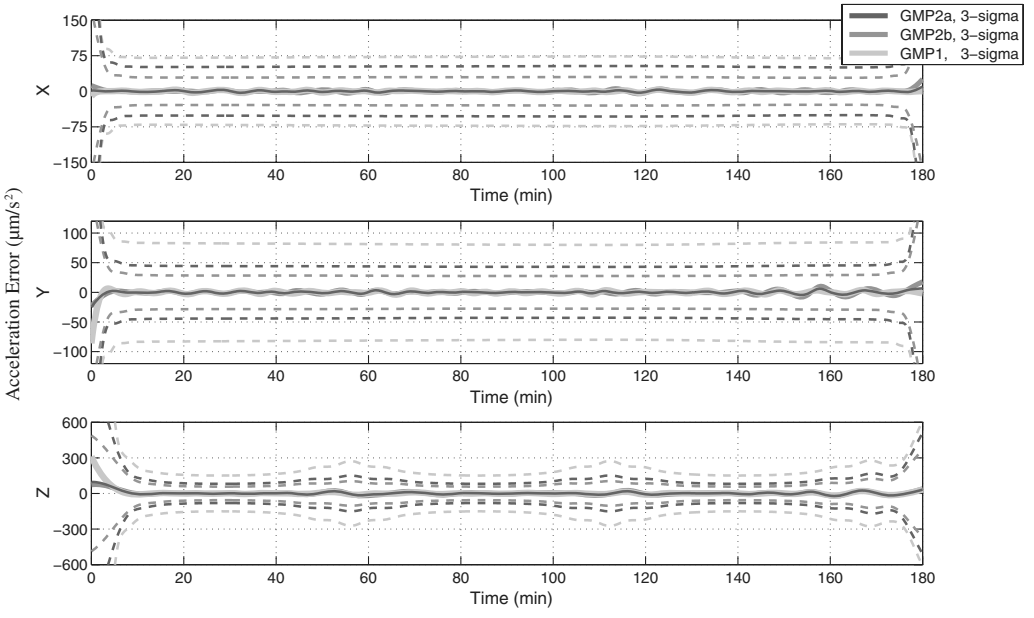

Fig. 11 Case 2 ECI acceleration for fully observed smoothed run.

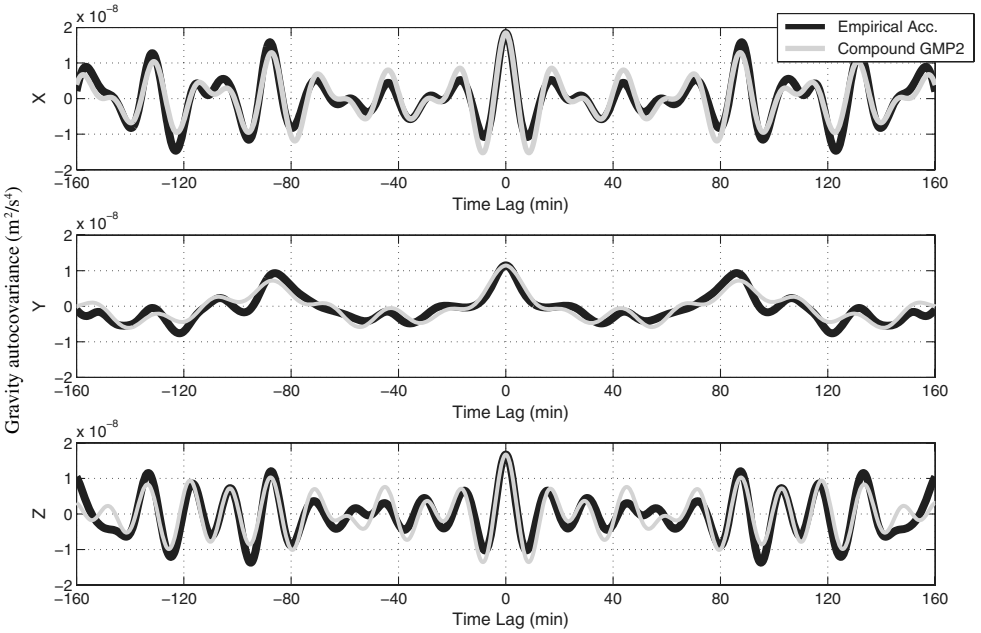

Fig. 12 Compound GMP2: ECI acceleration autocovariance (black) with compound GMP2 fit (gray).

coordinates. Again, the Y coordinate of GMP2b is limited by the autocovariance fit near the origin.

Case 2 is then backward smoothed to determine how well the unmodeled accelerations could be recovered. Here, the uncertainty envelopes are included to show that all of the errors fall within the uncertainty envelopes. Actual uncertainties are on the order of $\sim$75 μm/s^2 for X, $\sim$50 μm/s^2 for Y, and $\sim$200 μm/s^2 for Z for all of the GMP processes. Figure 11 shows the smoother results for the fully observed case 2 filter run. All three methods recover the unmodeled accelerations rather well, whereas GMP2b is the worst in the Y coordinate. Table 8 displays the statistics for the smoothing run. One can see that smoothing has greatly increased the recovery of unmodeled accelerations for case 2 as well.

For both cases, a single well-calibrated Gauss-Markov process (GMP2a) outperformed the first order process (GMP1) and a poorly calibrated second order process (GMP2b). These results are seen for both continuous observations and poor tracking for a forward filtered solution. Smoothed filter results demonstrated an improvement in the solution for both GMP1 and GMP2. Fully observed GMP2 results were very similar or worse than GMP1. The degraded performance is most likely due to the increased statistical degree of freedom of GMP2. A comparison of the filtered and smoothed results for the two cases analyzed is presented in Table 9.

Table 8 Case 2 fully observed period smoothed rms values[a]

	Position, m			Acceleration, μm/s^2		
	GMP1	GMP2a	GMP2b	GMP1	GMP2a	GMP2b
X	0.017	0.017	0.025	1.33	1.34	3.00
Y	0.017	0.018	0.028	1.69	1.83	3.28
Z	0.160	0.200	0.262	6.92	8.71	10.72
R	0.162	0.202	0.264	7.25	9.00	11.61

[a]Root mean square values are computed from the difference between smoothed estimates and true ECI unmodeled accelerations.

Table 9 Comparison of GMP2 vs. GMP1[a]

	Case 1		Case 2	
	GMP2a	GMP2b	GMP2a	GMP2b
Fully observed filtered	Better	Better	Better	Worse
Partially observed filtered	Better	Better	Better	Worse
Fully observed smoothed	Similar	Similar	Worse	Worse

[a]Criteria was determined from the percent change in rms values ($\text{rms}_{\text{GMP2}} - \text{rms}_{\text{GMP1}}$)/$\text{rms}_{\text{GMP1}}$ where "Better" is when the value is less than 10%, "Worse" is greater than 10%, and "Similar" is between -10% and 10%.

C. Compound GMP2

As seen in the preceding section, an optimal autocovariance fit is necessary to accurately estimate and predict unmodeled accelerations. Here the use of multiple GMP2s is attempted to achieve an optimal fit for the autocovariance as seen in Fig. 4. Figure 12 shows an autocovariance fit of three compounded GMP2s. The three GMP2s are all of sinusoidal and oscillatory properties, in which the final GMP2 is forced to complete the autocovariance fit near the origin. The filter performance resulting from the utilization of such a more complete autocovariance fit should be fully assessed in the future.

VI. Conclusions

Empirical accelerations are commonly modeled with two extreme types of autocovariance models in precise orbit determination: pure exponential decay or pure sinusoidal oscillation. A second-order Gauss–Markov process (GMP) offers an autocovariance model that is more flexible to fit against a wide variety of observed empirical behaviors. However, a trade-off may be necessary when one is attempting to fit a second-order Gauss–Markov process autocovariance to that of an empirical acceleration. One must not overfit the autocovariance in an attempt to obtain major frequencies at the expense of an optimal fit for small time lags. In other words, an autocovariance model that sustains oscillations at large time lags, instead of just dying off to zero, is a strong stochastic constraint that can be used to mitigate unobservability under poor tracking conditions. It must be used with restraint though, for it may bias the filtering results in case the autocovariance calibration is inaccurate.

An illustration of the autocovariance model calibration, that is, the procedure by which the coefficients of the autocovariance model (assumed known during the filter run) are obtained was given. The method described how calibration can be accomplished following a three-step procedure and discussed in more depth what are considered the most difficult steps, namely, how to obtain samples of the unknown acceleration. Some of the challenges involved in

bootstrapping the GMP calibration based on a preliminary filtering of the tracking data were highlighted. Although admittedly limited, this latter part of the investigation indicated the importance of backward smoothing in the preliminary run and also suggested the need for a physical justification for the degree of continuity near the origin.

Improvements in precise orbit determination filtering have been demonstrated through the use of a second-order Gauss–Markov process for modeling gravitational accelerations beyond J_2 that were unmodeled in the filter dynamic model. Two cases have been analyzed in which empirical acceleration autocovariances are highly variable. In both cases, the use of a single well-calibrated second-order Gauss–Markov process (GMP2a) outperformed a first-order Gauss–Markov process (GMP1) and a poorly calibrated second-order Gauss–Markov process (GMP2b) for both continuous observations and poor tracking data when filtering forward.

Smoothed filter results demonstrated improved solutions for both the first- and second-order Gauss–Markov processes. In both cases examined, fully observed smoothed results for the second-order Gauss–Markov process were either very similar or worse when compared with the smoothed results for the first-order Gauss–Markov process. This degraded performance is most likely due to the increased statistical degree of freedom of the second-order Gauss–Markov process and thus the solution can become degraded due to the estimation of more parameters.

It must be emphasized that an unrestrained autocovariance fit (GMP2b) has the potential to be more useful than a restrained one (GMP2a) when observations are sparse. However, an unrestrained autocovariance fit may also cause damage if it is inaccurate. In the case of dense observations, in which the system dynamics are already well constrained by the observations alone, it is advisable to avoid the risk of an inaccurate fit and adopt a more restrained autocovariance fit.

Through the use of Gauss–Markov processes, increased filter performance led to more accurate estimates of the satellites position and acceleration having implications for gravity mapping missions, such as the Challenging Minisatellite Payload, the Gravity Recovery and Climate Experiment, or the Gravity Field and Steady-State Ocean Circulation Explorer, as well as other science missions requiring precise orbit determination solutions. Through the use of a sequential filter and smoother, properly calibrated Gauss–Markov processes have been shown to recover unmodeled accelerations better than a single sequential filter run.

Appendix A: Derivation

There are two approaches to obtaining a solution to the theory of Gaussian random processes. The first is the method of Fokker–Planck or the diffusion equation method. The second pays attention to the actual random variation in time of system variables one is interested in. Here the second is followed. It is convenient to develop the interested variables in a Fourier time series of which the variable coefficients can vary in a random fashion. One of the basic theorems is the fundamental notion of the spectrum of the random process and the connection between the spectrum and correlation functions. Follow closely the derivation presented by [15,18].

Suppose that there is a second-order differential equation that can be expressed in state vector notation as

$$\begin{bmatrix}\dot{x}_1\\ \dot{x}_2\end{bmatrix}=\begin{bmatrix}0 & 1\\ -\omega_n^2 & -2\zeta\omega_n\end{bmatrix}\begin{bmatrix}x_1\\ x_2\end{bmatrix}+\begin{bmatrix}0\\ c\end{bmatrix}w(t) \tag{A1}$$

with a forcing function $w(t)$, which is a Gaussian random process with moments

$$\mathrm{E}\{w(t)\}=0,\qquad \mathrm{E}\{w(t)w(t+\tau)\}=q\delta(\tau) \tag{A2}$$

The spectral density of $w(t)$ is the Fourier transform of the correlation function

$$S_w(\omega)=\int_{-\infty}^{\infty}\mathrm{d}t e^{i\omega t}\mathrm{E}\{w(t)w(0)\}=q \tag{A3}$$

which is white noise of strength q. Taking the Fourier transform of the state equations,

$$\begin{bmatrix}-i\omega x_1(\omega)\\ -i\omega x_2(\omega)\end{bmatrix}=\begin{bmatrix}0 & 1\\ -\omega_n^2 & -2\zeta\omega_n\end{bmatrix}\begin{bmatrix}x_1(\omega)\\ x_2(\omega)\end{bmatrix}+\begin{bmatrix}0\\ c\end{bmatrix}w(\omega) \tag{A4}$$

then $x_1(\omega)$ can be solved for in terms of the fluctuating force to obtain

$$x_1(\omega)=\frac{cw(\omega)}{\omega_n^2-\omega^2-(2\zeta\omega_n)i\omega} \tag{A5}$$

The spectral density of x_1 is proportional to $|x_1(\omega)|^2$ and so

$$S_{x_1}(\omega)=\frac{c^2S_w(\omega)}{|\omega_n^2-\omega^2-(2\zeta\omega_n)i\omega|^2}=\frac{c^2q}{(\omega_n^2-\omega^2)^2+(2\zeta\omega_n)^2\omega^2} \tag{A6}$$

For the corresponding time-dependent autocovariance function, one obtains

$$\Psi_{nn}(\tau)=\frac{1}{2\pi}\int_{-\infty}^{\infty}\mathrm{d}\omega e^{-i\omega t}S_{x_1}(\omega) \tag{A7}$$

$$\Psi_{nn}(\tau)=\frac{qc^2}{4\omega_n^3\zeta}e^{-\zeta\omega_n|\tau|}\left\{\cos\beta|\tau|+\frac{\zeta\omega_n}{\beta}\sin\beta|\tau|\right\} \tag{A8}$$

Next, the covariance matrix $\bar{\mathbf{P}}_s$ for purely a GMP2 (not the augmented system) is defined by

$$\begin{aligned}\bar{\mathbf{P}}_s(t)&=\Phi_s(t,t_0)\mathbf{P}_s(t_0)\Phi_s^{\mathrm{T}}(t,t_0)\\&\quad+\int_{t_0}^{t}\Phi_s(t,t')\mathbf{B}_s(t')\mathbf{Q}_s(t')\mathbf{B}_s^{\mathrm{T}}(t')\Phi_s^{\mathrm{T}}(t,t')\,\mathrm{d}t'\end{aligned} \tag{A9}$$

where the state transition matrix for Eq. (A1) is easily obtained:

$$\Phi_s(t)=e^{-\zeta\omega_n t}\begin{bmatrix}\cos\beta t+\frac{\zeta\omega_n}{\beta}\sin\beta t & \frac{1}{\beta}\sin\beta t\\ -\frac{\omega_n^2}{\beta}\sin\beta t & \cos\beta t-\frac{\zeta\omega_n}{\beta}\sin\beta t\end{bmatrix} \tag{A10}$$

with $\beta=\omega_n\sqrt{1-\zeta^2}$. Using $\mathbf{B}_s(t')=[0,c]^{\mathrm{T}}$ and solving for $\bar{\mathbf{P}}_s(t)$ yields

$$\begin{aligned}\bar{P}_{s_{11}}(t)&=e^{-2\zeta\omega_n t}\left[\left(\cos\beta t+\frac{\zeta\omega_n}{\beta}\sin\beta t\right)^2\bar{P}_{s_{11}}(0)\ldots\right.\\&\quad\left.+\frac{2}{\beta}\sin\beta t\left(\cos\beta t+\frac{\zeta\omega_n}{\beta}\sin\beta t\right)\bar{P}_{s_{12}}(0)+\frac{1}{\beta^2}\sin^2\beta t\bar{P}_{s_{22}}(0)\right]\ldots\\&\quad+\frac{qc^2}{4\omega_n^3\zeta}\left[1-\frac{e^{-2\zeta\omega_n t}}{\beta^2}(\omega_n^2-\zeta^2\omega_n^2\cos2\beta t+\zeta\omega_n\beta\sin2\beta t)\right]\end{aligned} \tag{A11}$$

$$\begin{aligned}\bar{P}_{s_{12}}(t)&=e^{-2\zeta\omega_n t}\left[-\frac{\omega_n^2}{\beta}\sin\beta t\left(\cos\beta t+\frac{\zeta\omega_n}{\beta}\sin\beta t\right)\bar{P}_{s_{11}}(0)\ldots\right.\\&\quad+\left(\cos^2\beta t-\frac{1+\zeta^2}{1-\zeta^2}\sin^2\beta t\right)\bar{P}_{s_{12}}(0)\ldots\\&\quad\left.+\frac{1}{\beta}\sin\beta t\left(\cos\beta t-\frac{\zeta\omega_n}{\beta}\sin\beta t\right)\bar{P}_{s_{22}}(0)\right]\ldots\\&\quad+\frac{qc^2}{2\beta^2}e^{-2\zeta\omega_n t}\sin^2\beta t\end{aligned} \tag{A12}$$

$$\bar{P}_{s_{22}}(t) = e^{-2\zeta\omega_n t}\left[\frac{\omega_n^2}{1-\zeta^2}(\sin^2\beta t)\bar{P}_{s_{11}}(0)\ldots - \frac{2\omega_n^2}{\beta}\sin\beta t\left(\cos\beta t - \frac{\zeta\omega_n}{\beta}\sin\beta t\right)\bar{P}_{s_{12}}(0)\ldots + \left(\cos\beta t - \frac{\zeta\omega_n}{\beta}\sin\beta t\right)^2\bar{P}_{s_{22}}(0)\right]\ldots + \frac{qc^2}{4\omega_n\zeta}\left[1 - \frac{e^{-2\zeta\omega_n t}}{\beta^2}(\omega_n^2 - \zeta^2\omega_n^2\cos 2\beta t + \zeta\omega_n\beta\sin 2\beta t)\right] \tag{A13}$$

From the solutions given in Eqs. (A11–A13), the correlation matrix can be obtained for the statistically stationary state and is given by

$$\begin{bmatrix}\Psi_{11} & \Psi_{12}\\ \Psi_{21} & \Psi_{22}\end{bmatrix} = \frac{qc^2}{4\omega_n^3\zeta}e^{-\zeta\omega_n|\tau|}\begin{bmatrix}\cos\beta|\tau| + \frac{\zeta\omega_n}{\beta}\sin\beta|\tau| & \frac{\omega_n^2}{\beta}\sin\beta|\tau|\\ \frac{\omega_n^2}{\beta}\sin\beta|\tau| & \cos\beta|\tau| - \frac{\zeta\omega_n^3}{\beta}\sin\beta|\tau|\end{bmatrix} \tag{A14}$$

For $\mathrm{E}\{x_s^2(t)\} = \sigma^2$ as $t \to \infty$, the desired value of c^2 is

$$c^2 = \frac{4\omega_n^3\zeta\sigma^2}{q} \tag{A15}$$

Appendix B: Implementation

This section assists the interested reader in implementing the preceding model into a sequential Kalman filter and briefly describes the structure of the main matrices and vectors involved. This is an extension of the implementation presented in [17]. Let the position vector of the satellite state in three-dimensional space be defined as $\mathbf{r} = [\,x \quad y \quad z\,]^{\mathrm{T}}$ and let the velocity vector be $\dot{\mathbf{r}} = [\,\dot{x} \quad \dot{y} \quad \dot{z}\,]^{\mathrm{T}}$. The satellite state $\mathbf{X}$ contains the position and velocity vectors as well as p parameters describing drag, gravity, etc., defined by $\boldsymbol{\beta}$, where

$$\mathbf{X} = \begin{bmatrix}\mathbf{r}^{\mathrm{T}} & \dot{\mathbf{r}}^{\mathrm{T}} & \boldsymbol{\beta}^{\mathrm{T}}\end{bmatrix}^{\mathrm{T}} \tag{B1}$$

The shaping-filter state vector $\mathbf{X}_s$ is made up of two vectors, $\mathbf{X}_{s_1}$ and $\mathbf{X}_{s_2}$, each with three spatial dimensions:

$$\mathbf{X}_s = [\,\mathbf{X}_{s_1}^{\mathrm{T}} \quad \mathbf{X}_{s_2}^{\mathrm{T}}\,]^{\mathrm{T}} = [\,X_{s_1x} \quad X_{s_1y} \quad X_{s_1z} \quad X_{s_2x} \quad X_{s_2y} \quad X_{s_2z}\,]^{\mathrm{T}} \tag{B2}$$

The augmented state vector can then be defined as $\mathbf{X}_a = [\,\mathbf{X}^{\mathrm{T}} \quad \mathbf{X}_s^{\mathrm{T}}\,]^{\mathrm{T}}$ with a state rate vector given as

$$\dot{\mathbf{X}}_a = \begin{bmatrix}\dot{\mathbf{r}}_a^{\mathrm{T}} & \ddot{\mathbf{r}}_a^{\mathrm{T}} & \dot{\boldsymbol{\beta}}^{\mathrm{T}} & \mathbf{X}_{s_2}^{\mathrm{T}} & (-\boldsymbol{\omega}_n^2 \circ \mathbf{X}_{s_1} - 2\boldsymbol{\zeta}\circ\boldsymbol{\omega}_n\circ\mathbf{X}_{s_2})^{\mathrm{T}}\end{bmatrix}^{\mathrm{T}} \tag{B3}$$

Notice that there can be three spatial dimensions given to the GMP2 parameter vectors $\boldsymbol{\sigma}, \boldsymbol{\omega}_n$, and $\boldsymbol{\zeta}$, for example $\boldsymbol{\zeta} = [\,\zeta_x \quad \zeta_y \quad \zeta_z\,]^{\mathrm{T}}$; in other words, a separate GMP2 process is used for each coordinate. The operation $\boldsymbol{\zeta}\circ\boldsymbol{\omega} = [\,\zeta_x\omega_{nx} \quad \zeta_y\omega_{ny} \quad \zeta_z\omega_{nz}\,]^{\mathrm{T}}$ is the element-wise product of two vectors. Vector exponentiation is defined elementwise: $\boldsymbol{\omega}^2 = [\,\omega_{nx}^2 \quad \omega_{ny}^2 \quad \omega_{nz}^2\,]^{\mathrm{T}}$. Augmented accelerations are thus defined as $\ddot{\mathbf{r}}_a = \ddot{\mathbf{r}} + \ddot{\mathbf{r}}_s$ where $\ddot{\mathbf{r}}$ are the deterministic dynamic model accelerations (i.e., gravity, atmospheric drag, etc.) and $\ddot{\mathbf{r}}_s$ are the empirical accelerations from the shaping filter output $\ddot{\mathbf{r}}_s = \mathbf{X}_{s_1}$. The augmented velocities are defined as $\dot{\mathbf{r}}_a$ and are simply related to the integration of $\ddot{\mathbf{r}}_a$.

The $\mathbf{A}_a(t)$ matrix is the Jacobian of the augmented state rate with respect to the augmented state and has the following partitioning:

$$\mathbf{A}_a(t) = \begin{bmatrix}\mathbf{A}(t) & \mathbf{B}(t)\tilde{\mathbf{H}}_s(t)\\ \mathbf{0}_{6\times(6+p)} & \mathbf{A}_s(t)\end{bmatrix} = \begin{bmatrix}\mathbf{0} & \mathbf{I} & \frac{\partial\ddot{\mathbf{r}}}{\partial\boldsymbol{\beta}} & \mathbf{0} & \mathbf{0}\\ \frac{\partial\ddot{\mathbf{r}}}{\partial\mathbf{r}} & \frac{\partial\ddot{\mathbf{r}}}{\partial\dot{\mathbf{r}}} & \frac{\partial\ddot{\mathbf{r}}}{\partial\boldsymbol{\beta}} & \mathbf{I} & \mathbf{0}\\ \frac{\partial\dot{\boldsymbol{\beta}}}{\partial\mathbf{r}} & \frac{\partial\dot{\boldsymbol{\beta}}}{\partial\dot{\mathbf{r}}} & \frac{\partial\dot{\boldsymbol{\beta}}}{\partial\boldsymbol{\beta}} & \mathbf{0} & \mathbf{0}\\ \mathbf{0} & \mathbf{0} & \mathbf{0}_{3\times p} & \mathbf{I} & \mathbf{0}\\ \mathbf{0} & \mathbf{0} & \mathbf{0}_{3\times p} & -\mathrm{diag}(\boldsymbol{\omega}_n\circ\boldsymbol{\omega}_n) & -2\mathrm{diag}(\boldsymbol{\zeta}\circ\boldsymbol{\omega}_n)\end{bmatrix} \tag{B4}$$

Except where noted, the identity matrix $\mathbf{I}$ and null matrix $\mathbf{0}$ have the dimensions 3×3. The matrix $\tilde{\mathbf{H}}_s(t) = [\,\mathbf{I} \quad 0\,]^{\mathrm{T}}$, which comes from $\mathbf{X}_{s_1}$, being the shaping filter output. The matrix $\mathbf{B}(t) = [\,\mathbf{0} \quad \mathbf{I} = \partial\ddot{\mathbf{r}}_s/\partial\mathbf{X}_{s_1} \quad \mathbf{0}_{p\times 3}\,]^{\mathrm{T}}$ comes from $\mathbf{X}_{s_1}$, being the acceleration in the same coordinate as $\ddot{\mathbf{r}}_s$.

The augmented $\tilde{\mathbf{H}}_a(t)$ matrix is the Jacobian of the observations with respect to the augmented state and is simply

$$\tilde{\mathbf{H}}_a(t) = \begin{bmatrix}\tilde{\mathbf{H}}(t) & \mathbf{0}_{m\times 6}\end{bmatrix}^{\mathrm{T}} \tag{B5}$$

where none of the m scalar range and range-rate observations depend on the empirical accelerations. The exact formulation of $\tilde{\mathbf{H}}(t)$ is dependent upon the types of observations processed. The matrix $\mathbf{B}_a(t)$ is the Jacobian of the state rate with respect to the white noise and is given as

$$\mathbf{B}_a(t) = \begin{bmatrix}\mathbf{0}_{(6+p)\times 3}\\ \mathbf{B}_s(t)\end{bmatrix} = \begin{bmatrix}\mathbf{0}_{(6+p)\times 3}\\ \mathbf{0}\\ \mathrm{diag}(\mathbf{c})\end{bmatrix} \tag{B6}$$

where c is determined from Eq. (A15).

The state-transition matrix $\Phi_a(t, t_0)$ can be obtained from numerical integration of $\mathbf{A}_a(t)$ with the initial conditions $\Phi_a(t_0, t_0) = \mathbf{I}$. An efficient seventh-order Runge–Kutta–Fehlberg RKF7(8) algorithm is used to numerically integrate Φ_a. One may also use the analytical expressions for the Φ matrix as seen in Eq. (A10).

The time-updated state covariance matrix can be obtained two different ways. The first is numerical integration of Eq. (18). The other is for the discrete case given in Eq. (19), in which the covariance matrix can be broken up into two terms: $\bar{\mathbf{P}}_a = \bar{\mathbf{P}}'_a + \bar{\mathbf{P}}''_a$; the first term is simply $\bar{\mathbf{P}}'_a = \Phi_a\mathbf{P}_a\Phi_a^{\mathrm{T}}$; and the second term is

$$\bar{\mathbf{P}}''_a = \mathbf{B}_d(t_0)\mathbf{Q}_d(t_0)\mathbf{B}_d^{\mathrm{T}}(t_0) = \mathbf{B}_d(t_0)[\mathbf{B}_a(t_0)\mathbf{Q}_a(t_0)\mathbf{B}_a^{\mathrm{T}}(t_0)\times(t-t_0)]\mathbf{B}_d^{\mathrm{T}}(t_0) \tag{B7}$$

Some simplifications for this case can be made as discussed in [16], in which one can postulate that $\mathbf{B}_{\mathrm{d}} = \mathbf{I}$, $\mathbf{Q}_a = \mathbf{I}$, resulting in

$$\bar{\mathbf{P}}''_a = \begin{bmatrix}\mathbf{0}_{(6+p)\times(6+p)} & \mathbf{0}_{(6+p)\times 3} & \mathbf{0}_{(6+p)\times 3}\\ \mathbf{0}_{3\times(6+p)} & \mathbf{0} & \mathbf{0}\\ \mathbf{0}_{3\times(6+p)} & \mathbf{0} & \mathrm{diag}(\mathbf{c}\circ\mathbf{c})\end{bmatrix}\times|t-t_0| \tag{B8}$$

where the absolute value surrounding the time lag is necessary when running the filter in a backward manner, such as a sequential smoother. It must be emphasized that Eqs. (B6) and (B7) are first-order approximations and are only valid if the system model is time invariant or slowly varying. If the system is not time invariant or slowly varying, an analytical solution or numerical integration of Eq. (18) is necessary. It may also be necessary to obtain an analytical solution or numerical integration of Eq. (18) if one is making future predictions in which time lags are considerably large.

Acknowledgment

Felipe G. Nievinski acknowledges funding provided by Fulbright/Capes.

References

[1] Luthcke, S., Zelensky, N., Rowlands, D., Lemoine, F., and Williams, T., "The 1-Centimeter Orbit: Jason-1 Precision Orbit Determination Using

GPS, SLR, DORIS, and Altimeter Data Special Issue: Jason-1 Calibration/Validation," *Marine Geodesy*, Vol. 26, No. 3, 2003, pp. 399–421.
doi:10.1080/714044529

[2] Wu, S., Yunck, T., and Thornton, C., "Reduced-Dynamic Technique for Precise Orbit Determination of Low Earth Satellites," *Astrodynamics 1987*, Vol. 1, Univelt, San Diego, CA, 1988, pp. 101–113.

[3] Montenbruck, O., Van Helleputte, T., Kroes, R., and Gill, E., "Reduced Dynamic Orbit Determination Using GPS Code and Carrier Measurements," *Aerospace Science and Technology*, Vol. 9, No. 3, 2005, pp. 261–271.
doi:10.1016/j.ast.2005.01.003

[4] Marshall, J., Zelensky, N., Klosko, S., Chinn, D., Luthcke, S., Rachlin, K., and Williamson, R., "The Temporal and Spatial Characteristics of TOPEX/POSEIDON Radial Orbit Error," *Journal of Geophysical Research*, Vol. 100, No. C12, 1995, pp. 25,331–25,352.
doi:10.1029/95JC01845

[5] Myers, K., and Tapley, B., "Dynamical Model Compensation for Near-Earth Satellite Orbit Determination," *AIAA Journal*, Vol. 13, March 1975, pp. 343–349.
doi:10.2514/3.49702

[6] Bierman, G., *Factorization Methods for Discrete Sequential Estimation*, Vol. 128. Academic Press, New York, 1977, pp. 135–136 and 150–152.

[7] Tapley, B., Schutz, B., and Born, G., *Statistical Orbit Determination.*, Academic Press, New York, 2004, pp. 220–233.

[8] Wright, J., "Sequential Orbit Determination with Auto-Correlated Gravity Modeling Errors," *Journal of Guidance, Control, and Dynamics*, Vol. 4, No. 3, 1981, pp. 304–309.
doi:10.2514/3.56083

[9] Wright, J., Woodburn, J., Truong, S., and Chuba, W., "Orbit Gravity Error Covariance," *18th AAS/AIAA Space Flight Mechanics Meeting*, American Astronautical Society Paper 08-157, Jan. 2008.

[10] Wright, J., Woodburn, J., Truong, S., and Chuba, W., "Sample Orbit Covariance Function and Filter-Smoother Consistency Tests," *18th AAS/AIAA Space Flight Mechanics Meeting*, American Astronautical Society Paper 08-159, Jan. 2008.

[11] Wright, J., Woodburn, J., Truong, S., and Chuba, W., "Orbit Covariance Inner Orbit Covariance Inner Integrals with Polynomials," *18th AAS/AIAA Space Flight Mechanics Meeting*, American Astronautical Society Paper 08-161, Jan. 2008.

[12] Beutler, G., Jäggi, A., Mervart, L., and Meyer, U., "The Celestial Mechanics Approach: Application to Data of the GRACE Mission," *Journal of Geodesy*, Vol. 84, No. 11,2010, pp. 661–681.
doi:10.1007/s00190-010-0402-6

[13] Nazarenko, A. I., and Alfriend, K. T., "Development of the Technique for Covariance Prediction Using the Gravity Color Noise," *AAS/AIAA Space Flight Mechanics Conference*, AAS 09-230, Univelt, Feb. 2009.

[14] Gelb, A., *Applied Optimal Estimation*, MIT Press, Cambridge, MA, 1974, pp. 42–45.

[15] Bryson, A., and Ho, Y., *Applied Optimal Control: Optimization, Estimation, and Control*, Hemisphere, New York, 1975, pp. 180–185.

[16] Maybeck, P., *Stochastic Models, Estimation and Control*, Vol. 141-1. Academic Press, Cambridge, MA, 1979, pp. 367–370.

[17] Nievinski, F. G., Yonko, B., and Born, G. H., "Improved Orbit Determination Using Second-Order Gauss–Markov Processes," *AAS/AAIA Space Flight Mechanics Meeting*, American Astronautical Society Paper 11-119, Feb. 2011.

[18] Wang, M., and Uhlenbeck, G., "On the Theory of the Brownian Motion II," *Reviews of Modern Physics*, Vol. 17, Nos. 2–3, 1945, pp. 323–342.
doi:10.1103/RevModPhys.17.323

[19] Fehlberg, E., *Classical Fifth-, Sixth-, Seventh-, and Eighth-Order Runge-Kutta Formulas with Stepsize Control*, Clearinghouse for Federal Scientific and Technical Information, Springfield, VA, 1968, p. 65.

[20] Tapley, B., Ries, J., Bettadpur, S., Chambers, D., Cheng, M., Condi, F., Gunter, B., Kang, Z., Nagel, P., Pastor, R., Pekker, T., Poole, S., and Wang, F., "GGM02—An Improved Earth Gravity Field Model from GRACE," *Journal of Geodesy*, Vol. 79, No. 8, 2005, pp. 467–478.
doi:10.1007/s00190-005-0480-z

[21] Gottlieb, R. G., "Fast Gravity, Gravity Partials, Normalized Gravity, Gravity Gradient Torque and Magnetic Field: Derivation, Code and Data," NASA CR 188243, 1993.

[22] Picone, J. M., Hedin, A., Drob, D., and Aikin, A., "NRLMSISE-00 Empirical Model of the Atmosphere: Statistical Comparisons and Scientific Issues," *Journal of Geophysical Research*, Vol. 107, No. A12, 2002, p. 1468.
doi:10.1029/2002JA009430

[23] Maybeck, P., *Stochastic Models, Estimation and Control*, Vol. 141-2. Academic Press, New York, 1979, p. 289.

[24] Kovačvić, B., and Durovic, Z., "*Fundamentals of Stochastic Signals, Systems and Estimation Theory with Worked Examples*," Springer–Verlag, New York, 2008, p. 380.

[25] Crassidis, J., and Junkins, J., *Optimal Estimation of Dynamic Systems.* Chapman and Hall, Boca Raton, FL, 2004, p. 591.

[26] Speyer, J., and Chung, W., *Stochastic Processes, Estimation, and Control*, Vol. 17. Society for Industrial and Applied Mathematics, Philadelphia, PA, 2008, p. 383.

[27] Orfanidis, S., *Optimum Signal Processing: An Introduction*, 2nd ed., Prentice–Hall, Upper Saddle River, NJ, 1996, p. 164.

D. Spencer
Associate Editor